

Supplemental Material

Titanium Substitutions in Garnet at Magmatic, Granulite Facies, and High-Pressure Granulite Facies Conditions

Jay J. Ague^{1,2}, Duncan S. Keller³, Michael R. Ackerson⁴, and Megan Holycross⁵

¹Department of Earth and Planetary Sciences, Yale University, PO Box 208109, New Haven, CT 06520-8109 U.S.A.

²Division of Mineralogy and Meteoritics, Yale Peabody Museum, Yale University, PO Box 208118, New Haven, CT 06520-8118, U.S.A.

³Department of Earth, Environmental and Planetary Sciences, Rice University, 6100 Main St. Houston, TX 77005 U.S.A.

⁴Department of Mineral Sciences, Smithsonian National Museum of Natural History, Washington DC 20560 U.S.A.

⁵Department of Earth and Atmospheric Sciences, Cornell University, Ithaca, NY 14850 U.S.A.

Additional Tests of Formula Normalization Procedures

As noted in the main text, the 2-octahedral-cation normalization could potentially overestimate Fe^{3+} in two main ways that involve $^{\text{VI}}\text{M}^{2+}$ and/or $^{\text{VI}}\text{Si}^{4+}$.

Majorite-type substitutions

Firstly, there is the ultrahigh-pressure (UHP) majorite substitution $^{\text{VI}}\text{Si}^{4+} + ^{\text{VI}}\text{M}^{2+} \leftrightarrow 2^{\text{VI}}\text{Al}^{3+}$, as well as its Ti analog $^{\text{VI}}\text{Ti}^{4+} + ^{\text{VI}}\text{M}^{2+} \leftrightarrow 2^{\text{VI}}\text{Al}^{3+}$ (Ringwood and Major, 1971). The vast majority of direct Mössbauer determinations of garnet Fe^{3+} and Fe^{2+} in the literature have been done on mantle xenoliths. Their P – T range is mostly outside of that considered herein and may extend into the realm of majorite-type substitutions ($> \sim 6$ GPa; e.g. Collerson et al. 2010; Wood et al. 2013). Many of these are ultramafic and, thus, are outside our compositional range as well.

Nonetheless, application of the 2-octahedral-cation method reveals some interesting systematics. For example, we consider two xenolith studies for which Mössbauer determinations of $\text{Fe}^{3+}/(\text{Fe}^{3+} + \text{Fe}^{2+})$ (denoted $\text{Fe}^{3+}/\Sigma\text{Fe}$) were made. One is Sobolev et al. (1999), which was designed to test how well Fe valences can be estimated via stoichiometry using electron-probe microanalyzer (EPMA) analyses (Fig. S1). The other comprises selected samples from Luth et al. (1990) and Canil and O'Neill (1996) which have new EPMA analyses done by M. E. Holycross as part of the Holycross et al. (2024) study (Table S1). Below, we refer to Sobolev et al. (1999) as S99, and Luth et al. (1990) and Canil and O'Neill (1996) as L90&CO96.

As shown in Figure S1a, the 2-octahedral-cation method performs very well for the S99 + new L90&CO96 analyses. Two analyses with elevated $\text{Fe}^{3+}/\Sigma\text{Fe}$ plot above the 1:1 correlation line, which could potentially reflect some degree of majorite-type substitutions. This is consistent with the fact that of those garnets with published P estimates, the highest P garnet plots farthest from the 1:1 line (5.65 GPa; BD 2501 in Luth et al. 1990). As garnet $\text{Fe}^{3+}/\Sigma\text{Fe}$ increases in a general way with P and T in Earth's mantle (e.g. Luth et al. 1990; Canil and O'Neill 1996; Woodland and Koch 2003), increases in majorite-type substitutions and $\text{Fe}^{3+}/\Sigma\text{Fe}$ could plausibly be coupled. Regardless, the 2-octahedral-cation method (Fig. S1a) still provides usable results and thus could be valuable for distinguishing trends in $\text{Fe}^{3+}/\Sigma\text{Fe}$ and redox state in xenolith suites.

In contrast, when the original analyses of L90&CO96 are used, the 2-octahedral-cation method yields substantially degraded results (Fig. S1b). This illustrates the well-known strong dependence of $\text{Fe}^{3+}/\Sigma\text{Fe}$ estimates on the major element EPMA analyses.

The 8-total-cation method for S99 + new L90&CO96 yields a positive correlation between the estimates of $\text{Fe}^{3+}/\Sigma\text{Fe}$ and the Mössbauer measurements, but the values are consistently overestimated (Fig. S1c). For the L90&CO96 EPMA analyses, the $\text{Fe}^{3+}/\Sigma\text{Fe}$ estimates made with the 8-total-cation method are very poor, as was previously recognized in the original studies (Fig. S1d).

We conclude that the two-octahedral-cation method can produce quantitative estimates of garnet $\text{Fe}^{3+}/\Sigma\text{Fe}$ when used in conjunction with modern EPMA analyses employing state-of-the-art wavelength-dispersive spectrometers, off-peak background corrections, and matrix corrections (Figs. 1a, 1c, S1a). Even with such analyses, however, the 8-total-cation method can yield much lower quality results, although it potentially might still reveal redox trends (Fig. S1b). Neither method performs particularly well if there are issues with the EPMA analyses; in particular, the 8-total-cation method yields estimates that are essentially useless in such cases (Fig. S1d).

Figure S1a suggests that some majorite-type substitutions may have operated in xenolith garnets with elevated $\text{Fe}^{3+}/\Sigma\text{Fe}$. This should be borne in mind whenever the 2-octahedral-cation method is used for xenolith assemblages. The range of $\text{Fe}^{3+}/\Sigma\text{Fe}$ in natural xenolith garnets extends up to ~ 0.16 . Thus, estimates that significantly exceed this (e.g. $> \sim 0.2$) should be regarded with considerable caution, regardless of the method used to calculate them.

Morimotoite substitution

The second possibility is the morimotoite substitution, identical in form to the Ti-analog majorite substitution ($^{\text{VI}}\text{Ti}^{4+} + ^{\text{VI}}\text{M}^{2+} \leftrightarrow 2^{\text{VI}}\text{Al}^{3+}$). The two are found in very different settings, however, as the Ti-analog majorite-type substitution occurs in relatively low-Ti, UHP ($> \sim 6$ GPa) garnets, whereas morimotoite operates in very Ti-rich andradites in, for example, skarns and alkaline igneous rocks. Such garnets are obviously far outside the composition range of interest. Mössbauer results are limited, but Pedrazzi et al. (2002) found the morimotoite contribution to be minor or absent in the three Ti-garnets they studied. Antao et al. (2015) found a larger role for morimotoite, but their results are based on the 8-total-cation normalization

scheme and furthermore do not consider OH, which can be considerable (e.g. Reynes et al. 2020). Although more work is necessary, our advice is to never use the 2-octahedral-cation method with Ti-rich andradite garnets owing to the possibility of the morimotoite substitution, as well as substitutions involving appreciable OH.

Evaluation of Experimental Garnets Using the 8-Total-Cation Method

As discussed in previous studies (e.g. Luth et al. 1990; Canil and O'Neill 1996; Sobolev et al. 1999) and shown in Figures 1d, S1b, and S1d, stoichiometric Fe^{3+} estimation methods employing all X, Y, and Z sites (which sum to 8 cations for ideal garnet) generally have low accuracy. Although the 8-total-cation method has the potential to reveal the operation of the Mmt substitution (but *only* in the absence of dodecahedral site vacancies), the highly scattered results of the method limit how much can be learned. For the experimental dataset compiled in this study, we find that modest filtering of the data can improve the scatter. To this end, we do not consider analyses that: (1) yield negative Fe^{3+} estimates and (2) have octahedral site totals ($^{\text{VI}}\text{Al} + \text{Ti} + \text{Fe}^{3+} + \text{Cr}^{3+}$) significantly exceeding 2.0 (we set the cutoff at > 2.005).

With these constraints, we can make some inferences about substitution mechanisms. Figure S2a shows the $^{\text{VI}}\text{Al}$ deficit versus Ti. The data form bands with slopes of ~ 1 which shift upward with increasing Fe^{3+} . This is the same relationship observed in Figure 3a in the main text computed using the 2-octahedral-cation method. In sharp contrast, the Mmt substitution predicts a steeper slope of 2. If the Adr substitution is allowed to introduce Fe^{3+} into the garnet, then the predicted compositional trend would move progressively upward into the top left corner of the graph. The data are, thus, inconsistent with any major contribution from Mmt.

Figure S2b depicts $^{\text{IV}}\text{Al}$ versus $^{\text{VI}}\text{Al}$. Once again, the same basic relationships obtained with the 2-cation procedure are evident (main text Fig. 3b), albeit with more scatter. The Mmt substitution, with or without Adr, predicts a linear trend that runs along the x -axis; there is no y -component as Mmt does not involve $^{\text{IV}}\text{Al}$. This is strongly at variance with the data, which clearly require $^{\text{IV}}\text{Al}$.

Figure S2c plots the total Al ($^{\text{T}}\text{Al}$) deficit – Fe^{3+} versus Ti and is color coded for garnet alkali content. As is the case for Figures S3a and S3b, the data follow the same basic pattern as observed for the 2-octahedral-cation method (main text Fig. 3c). This plot is particularly sensitive to the potential operation of the Mmt substitution, which would define a much steeper trend than observed. This is grossly inconsistent with the data.

Finally, we plot $^{\text{IV}}\text{Al} + \text{alkalis}$ versus Ti (Fig. S2d). First, this shows that the alkali systematics shown in the main text (Fig. 4) are evident regardless of formula normalization scheme. Thus, there is little doubt that coupled Ti – alkali substitution was operative. Second, as the Mmt substitution involves neither $^{\text{IV}}\text{Al}$ nor alkalis, its predicted trend lies along the x -axis, with no y -component. This is not compatible with the observed data array. We note that $^{\text{IV}}\text{Al} + \text{alkalis} + 2\Box$ versus Ti is not plotted (main text Fig. 4d), as the 8-total-cation scheme does not allow vacancies.

In summary, the Mmt substitution is unable to account for the major compositional trends in the experimental data, regardless of the formula normalization method used. If present, Mmt plays only a minor role (main text Fig. 5).

Evaluation of coupled Ts-Ti, Adr-Ti, and Adr substitutions

As discussed in the main text, the Ts-Ti, Adr-Ti, and Adr substitutions are not linearly independent, but we argue that a combination of all three provides the best description of the data. For example, this is well illustrated by the ^{VI}Al deficit versus Ti systematics shown in Figure S3.

References

- Antao, S. M., Mohib, S., Zaman, M., and Marr, R. A. (2015) Ti-rich andradites: Chemistry, structure, multi-phases, optical anisotropy, and oscillatory zoning. *The Canadian Mineralogist*, 53, 133-158.
- Canil, D., and O'Neill, H. S. C. (1996) Distribution of ferric iron in some upper-mantle assemblages. *Journal of Petrology*, 37, 609-635.
- Collerson, K. D., Williams, Q., Kamber, B. S., Omori, S., Arai, H., and Ohtani, E. (2010) Majoritic garnet: A new approach to pressure estimation of shock events in meteorites and the encapsulation of sub-lithospheric inclusions in diamond. *Geochimica et Cosmochimica Acta*, 74, 5939-5957.
- Holycross, M., and Cottrell, E. (2023) Garnet crystallization does not drive oxidation at arcs. *Science*, 380, 506-509.
- Holycross, M., Cottrell, E., Ague, J., Lanzirotti, A., and Newville, M. (2024) Fe K α XANES, Fe K β HERFD XANES and EPMA flank method determinations of the oxidation state of Fe in garnet. *Chemical Geology*, 647, 121937.
- Luth, R. W., Virgo, D., Boyd, F. R., and Wood, B. J. (1990) Ferric iron in mantle-derived garnets: Implications for thermobarometry and for the oxidation state of the mantle. *Contributions to Mineralogy and Petrology*, 104, 56-72.
- Pedrazzi, G., Schingaro, E., and Scordari, F. (2002) Mössbauer investigation on Ti-garnets from different geological environments. In *Hyperfine Interactions (C), Proceedings of the International Conference on the Applications of the Mössbauer Effect, (ICAME 2001) September 2–7, 2001, Oxford, UK (pp. 457-460)*. Dordrecht: Springer Netherlands.
- Reynes, J., Lanari, P., and Hermann, J. (2020) A mapping approach for the investigation of Ti–OH relationships in metamorphic garnet. *Contributions to Mineralogy and Petrology*, 175, 46, <https://doi.org/10.1007/s00410-020-01681-5>.

- Ringwood, A. E., and Major, A. (1971) Synthesis of majorite and other high pressure garnets and perovskites. *Earth and Planetary Science Letters*, 12, 411-418.
- Sobolev, V. N., McCammon, C. A., Taylor, L. A., Snyder, G. A., and Sobolev, N. V. (1999) Precise Mössbauer milliprobe determination of ferric iron in rock-forming minerals and limitations of electron microprobe analysis. *American Mineralogist*, 84, 78-85.
- Wood, B. J., Kiseeva, E. S., and Matzen, A. K. (2013) Garnet in the Earth's mantle. *Elements*, 9, 421-426.
- Woodland, A. B., and Koch, M. (2003) Variation in oxygen fugacity with depth in the upper mantle beneath the Kaapvaal craton, Southern Africa. *Earth and Planetary Science Letters*, 214, 295-310.

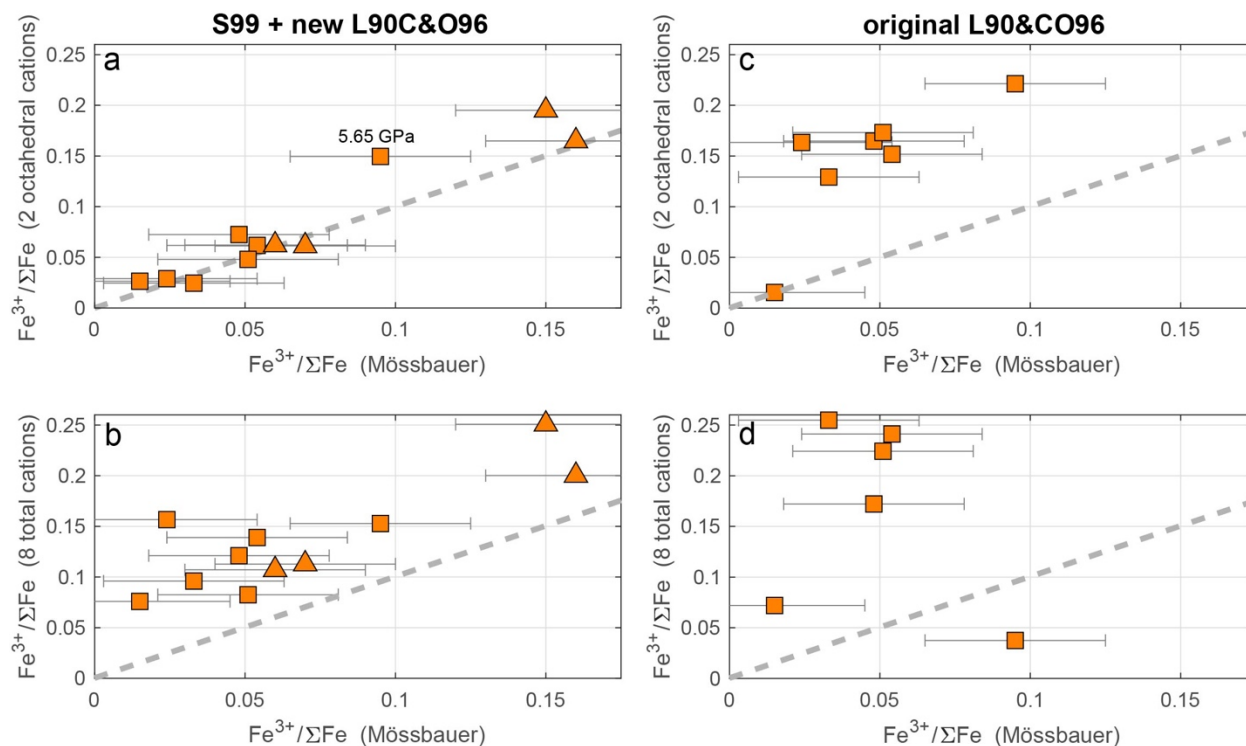


Figure S1. Comparison of the 2-octahedral-cation and 8-total-cation methods for the mantle xenolith data of Sobolev et al. (1999) (S99; triangles) and Luth et al. (1990) and Canil and O'Neill (1996) (L90&CO96; squares). The left panels use new EPMA analyses of representative L90&CO96 garnets (Holycross et al. 2024), whereas the right panels use the original analyses. In this and the following figures, estimates of Mossbauer uncertainty are from Holycross and Cottrell (2023). Dashed lines denote 1:1 correlation. (a), (c) Results for the 2-octahedral-cation method. (b), (d) Results for the 8-total-cation method. As shown in part (a), the 2-octahedral-cation method used together with the S99 + new L90&CO96 data provides the best results.

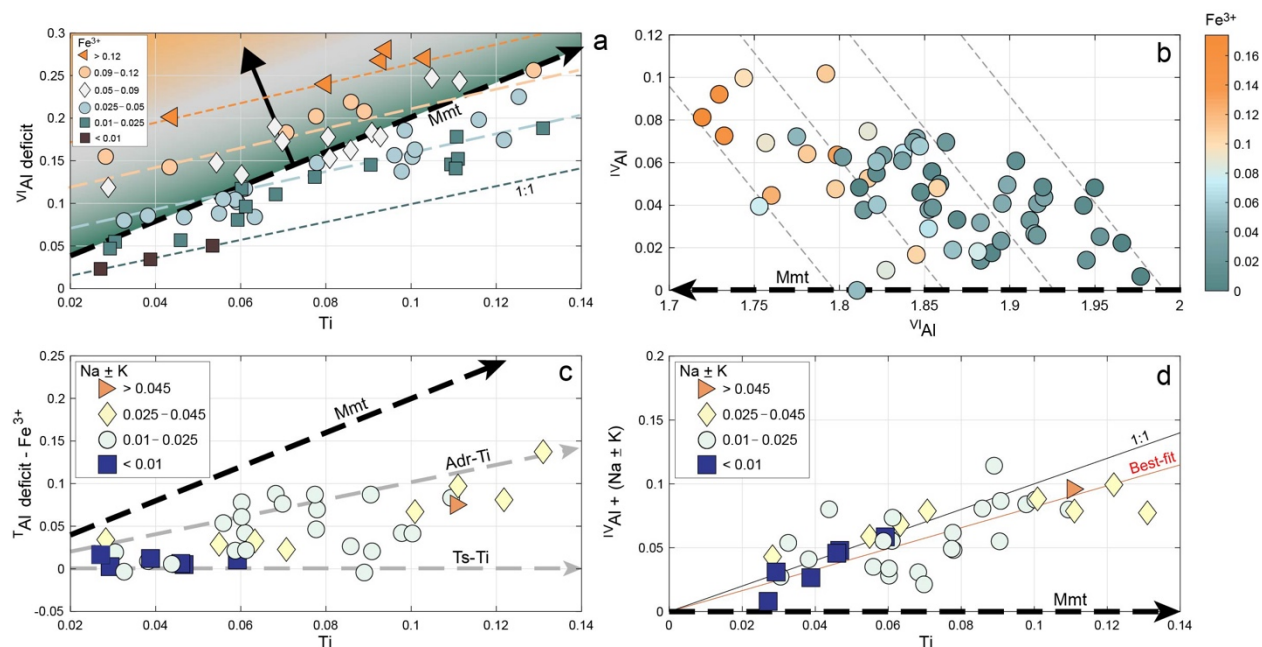


Figure S2. Garnet compositional systematics for the experimental data set of the main text computed using the 8-total-cation method. Mmt, Adr-Ti, and Ts-Ti denote the morimotoite, Andradite-Ti, and Tschermak-Ti substitutions, respectively. **(a)** ^{VI}Al deficit versus Ti color coded for Fe^{3+} content. Solid arrow shows direction of garnet compositional shift with increasing Fe^{3+} for coupled Mmt–Adr substitution, from low (dark green shading) to high (orange shading); shaded bands have the theoretical slope of 2 which is steeper than observed. **(b)** ^{IV}Al versus ^{VI}Al color coded for Fe^{3+} content. **(c)** Total Al (^{T}Al) deficit – Fe^{3+} versus Ti color coded for alkali content. **(d)** $^{IV}Al + (Na \pm K)$ versus Ti color coded for alkali content. In parts (b), (c), and (d), the Mmt trends are independent of any Adr substitution.

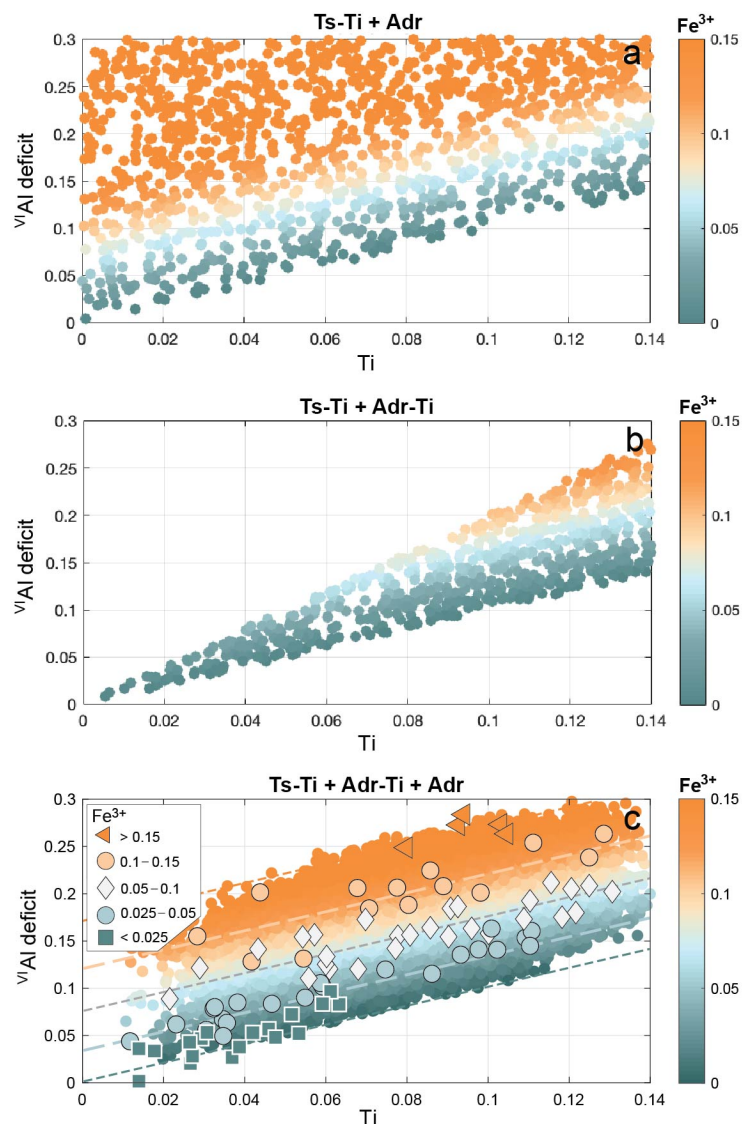


Figure S3. Monte Carlo tests of substitution mechanisms involving Fe^{3+} plotted on ^{VI}Al deficit versus Ti diagrams. Each color dot represents an individual Monte Carlo trial. **(a)** Coupled Ts-Ti and Adr substitutions. **(b)** Coupled Ts-Ti and Adr-Ti substitutions. **(c)** Coupled Ts-Ti, Adr-Ti, and Adr substitutions, as described in the text (main text Fig. 6a). The combination of all three substitutions in part (c) is most consistent with the experimental data (shown with symbols; 2-octahedral-cation method).